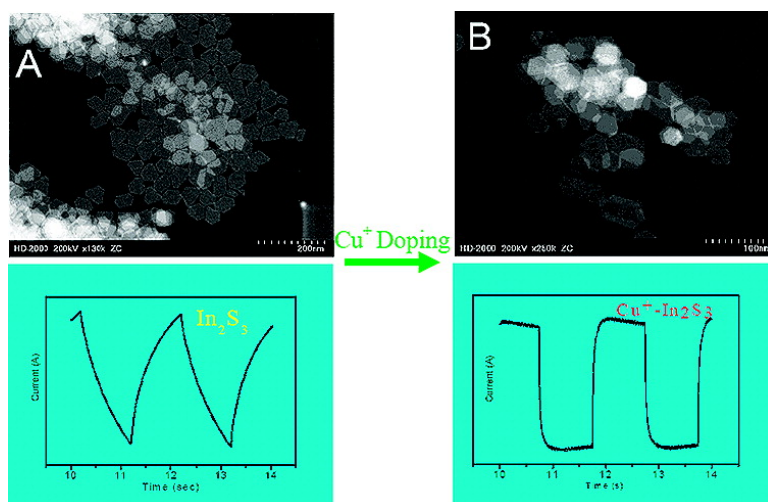# ACS NANO

Article

Heavy-Metal-Free Solution-Processed Nanoparticle-Based Photodetectors: Doping of Intrinsic Vacancies Enables Engineering of Sensitivity and Speed

Jiang Tang, Gerasimos Konstantatos, Sean Hinds, Stefan Myrskog, Andras G. Pattantyus-Abraham, Jason Clifford, and Edward H. Sargent

More About This Article

Additional resources and features associated with this article are available within the HTML version:

- Supporting Information
- Links to the 1 articles that cite this article, as of the time of this article download
- Access to high resolution figures
- Links to articles and content related to this article
- Copyright permission to reproduce figures and/or text from this article

View the Full Text HTML

ACS Publications
High quality. High impact.

Heavy-Metal-Free Solution-Processed Nanoparticle-Based Photodetectors: Doping of Intrinsic Vacancies Enables Engineering of Sensitivity and Speed

Jiang Tang,[†] Gerasimos Konstantatos,[‡] Sean Hinds,[‡] Stefan Myrskog,[‡] Andras G. Pattantyus-Abraham,[‡] Jason Clifford,[‡] and Edward H. Sargent[‡,*]

[†]Department of Materials Science and Engineering, 184 College Street, Toronto, Ontario M5S 3E4, and [‡]Department of Electrical and Computer Engineering, University of Toronto, 10 King's College Road, Toronto, Ontario M5S 3G4, Canada

ABSTRACT Photodetection in semiconductors enables digital imaging, spectroscopy, and optical communications. Integration of solution-processed light-sensing materials with a range of substrates offers access to new spectral regimes, the prospect of enhanced sensitivity, and compatibility with flexible electronics. Photoconductive photodetectors based on solution-cast nanocrystals have shown tremendous progress in recent years; however, high-performance reports to date have employed Pb- and Cd-containing materials. Here we report a high-sensitivity (photon-to-electron gain >40), high-speed (video-frame-rate-compatible) photoconductive photodetector based on In_2S_3. Only by decreasing the energetic depth of hole traps associated with intrinsic vacancies in beta-phase In_2S_3 were we able to achieve this needed combination of sensitivity and speed. Our incorporation of Cu^+ cations into beta-In_2S_3's spinel vacancies that led to acceptable temporal response in the devices showcases the practicality of incorporating dopants into nanoparticles. The devices are stable in air and under heating to 215 °C, advantages rooted in the reliance on the stable inclusion of dopants into available sites instead of surface oxide species.

KEYWORDS: indium sulfide · doping · intrinsic vacancy · solution-processed · photoconductive · photodetector

Digital imaging relies on arrays of individually read photodetectors. High signal-to-noise imaging at low light, combined with operation at video frame rates, requires sensitivity and speed simultaneously. In conventional photodiodes, in which the current collected is limited to one electron per photon incident, external quantum efficiency (EQE) is used as a proxy for sensitivity. Temporal response may be quantified through the longest time constant in a device's rise or fall in response to changes in illumination. EQEs approaching 100% (unity gain) are desired; while temporal responses faster than 100 ms are desired for video frame-rate lag-free imaging.

There is a growing interest[1−6] in integrating photosensitive layers on top of an electronic read-out circuit instead of relying on silicon's own sensitivity.[7] Whereas photodiodes are restricted to unity EQE, photoconductive photodetectors provide gains of 10-fold and above, thus providing many electrons for each photon incident. In conventional silicon CMOS imaging, photodiodes are buried beneath multiple micrometers of dielectric and metal interconnect, and they typically occupy less than half of the pixel area owing to sharing of silicon area with read-out circuitry. In contrast, top-surface photodetectors offer 100% fill factor.[8] Silicon's bandgap limits its applications to the visible and near-infrared, whereas the use of alternative top-surface photodetector materials makes possible imaging from the UV[9] through to the short-wavelength infrared.[1]

Promising recent reports of low-lag top-surface photoconductive photodetectors having the combination of good gain (>3) and acceptable temporal response (<100 ms)[10] have employed PbS colloidal quantum dots. More broadly, many recent advances in colloidal quantum dot electronics[11,12] and optoelectronics[13−15] have relied on the use of heavy-metal cations such as Cd and Pb that raise concerns regarding toxicity and regulatory acceptance.

Here we report Pb- and Cd-free photoconductive photodetectors. Our materials are based instead on indium sulfide (In_2S_3), a III_2-VI_3 semiconductor having a band gap of 2.03 eV.

As we report in detail below, employing this much less familiar colloidal nanoparticle materials system raised significant
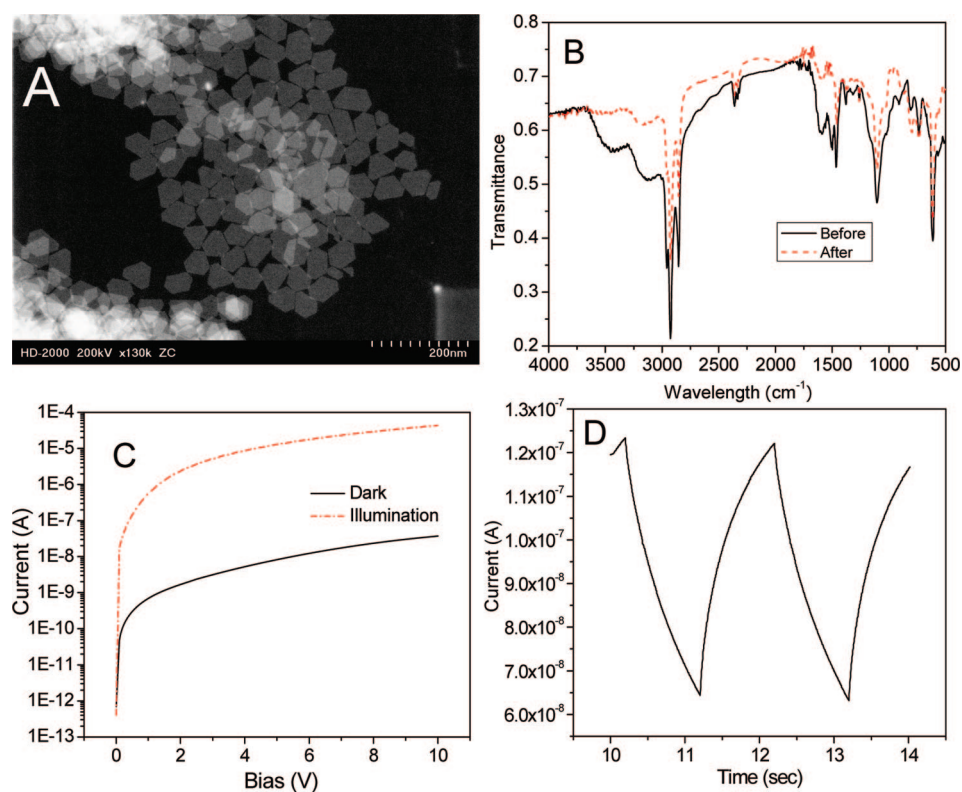
Figure 1. Materials and optoelectronic characteristics of In$_2$S$_3$ nanoplate photoconductive photodetectors: (A) scanning transmission electron microscopy (STEM) images of In$_2$S$_3$ nanoplates; (B) FTIR spectra of In$_2$S$_3$ nanoplates before and after 3-day butylamine ligand exchange; (C) current−voltage characteristics of In$_2$S$_3$ photodetector in the dark and under 470 nm light illumination at intensity of 7.4 μW/cm^2; (D) time-resolved photoresponse at optical intensity of 0.8 μW/cm^2.

but slow temporal response. Then we developed a one-pot postdoping strategy to introduce Cu$^+$ into In$_2$S$_3$ nanoplates in solution. Careful characterization of these materials confirmed the success of Cu$^+$ doping. An optimal level of Cu$^+$ doping greatly improved photodetector speed with little sacrifice of responsivity. These devices hold promise for high-sensitivity, video-frame-rate visible photodetector applications.

RESULTS

We first synthesized undoped In$_2$S$_3$ nanoplates and characterized the performance of devices made from such materials. In$_2$S$_3$ nanoplates were synthesized by heating InCl$_3$ and sulfur powder in oleylamine at 215 °C using a previously reported protocol.[19] As shown in Figure 1A, monodisperse In$_2$S$_3$ nanoplates were produced. The crystalline plates exhibit 6-fold symmetry with dimensions in the plane on the order of 30 nm. After synthesis and isolation, solution ligand exchange was employed to replace long oleylamine (∼2.4 nm) with short butylamine (∼0.6 nm) with the goal of increasing charge carrier mobility by reducing interparticle spacing. We used Fourier transform infrared spectroscopy (FTIR) to evaluate the effectiveness of this ligand exchange strategy. FTIR peaks (Figure 1b) of particular interest are the asymmetric and symmetric C−H stretching vibration of a CH$_2$ group at 2930 and 2857 cm^{-1}. Complete replacement of oleylamine by butylamine would produce a ∼4.5-fold decrease in the absorbance of these peaks. The observed 30% drop indicates partial replacement.

The ligand exchange procedure resulted in denser film (Figure S1) and improved carrier transport as evidenced by a 5 orders-of-magnitude increase in dark conductivity. Photoresponse was observed from the exchanged film, and thermal annealing significantly further increased photoresponse. Figure 1 panels C and D show device response following 10 min annealing in a vacuum oven. The device showed responsivity of 200 A/W, corresponding to a gain of greater than 500 electrons per incident photon. However, the temporal response of the device, seen in Figure 1D, exhibited time

challenges in making a photoconductive photodetector having attractive performance. Specifically, long-lived trap states, traceable to cationic vacancies associated with unoccupied indium tetrahedral positions in In$_2$S$_3$'s defect spinel structure (beta phase),[16] produced unacceptably long temporal responses in our first generation of devices.

In response we searched for a means of filling these vacant sites using metal ions. We found that the use of Cu cations allowed us to engineer the trap state lifetime to enable a desirable gain without the deleterious effects of excess lag. We note that these findings on doping overcome a longstanding problem in the colloidal nanocrystal field: self-purification, a consequence of the fact that the impurity solubility in small nanocrystals is much lower than in bulk materials.[17,18] We hypothesized that we could overcome such difficulties in achieving stable net doping by working with a material having intrinsic vacancies that would readily incorporate impurities if the size of impurity ion was compatible with the volume of vacancy; and if the affinity of the impurity ion was properly chosen.

As a consequence, we report herein a sensitive ($R > 10$ A/W) and fast ($\tau \sim 0.1$ s) solution-processed visible photodetector based on Cu$^+$-doped In$_2$S$_3$ nanoplates. We initially produced visible photodetectors, based on In$_2$S$_3$ nanoplates, having high responsivity

constants in the order of seconds.[9] Such speed is unacceptable for conventional imaging application because lag, or ghosting, will be perceptible in the image.

Motivated by previous reports of surface modification of nanoparticle-based films improving temporal response through the passivation of deep traps,[10] we investigated a variety of surface modifications. We attempted treatment with ethanethiol, ethanedithiol, formic acid, and methanol, and we also explored the use of annealing in different atmospheres (N_2, air, and vacuum) and at a number of temperatures (100−300 °C) (Figure S2). We additionally explored a variety of synthetic procedures such as the introduction of oleic acid (Figure S3) or TOP during the synthesis, use of different sulfur and indium sources, variations in In to S precursor ratios (Figure S4), and changes to growth temperature. Finally, we also explored a variety of handling procedures including isolation in ambient and different durations for the butylamine ligand exchange (Figure S5). Notably, all of these variants to the process failed to improve the temporal response of the photoconductive photodetectors while maintaining high responsivity (>1 A/W).

We tentatively concluded that manipulations to nanoparticle surfaces were not effective in improving temporal response. Physically, this could be explained if the deep trap states in these materials found their origins in the bulk, rather than the surface, properties of the crystals. In_2S_3 is a body-centered tetragonal compound with ordered vacancies. Indium atoms occupied all 24 octahedral sites and 8 tetrahedral sites in the unit cell, leaving 4 tetrahedral sites empty.[20] We posited that these vacancies inside—rather than on the surface of—the particle could be responsible for long-lived trapping, and would be unmodified by surface treatments alone.

In an effort to fill vacancies with metal ligands that would remove, or, more desirably, render more shallow the trap state energy, we investigated the incorporation of $CuCl_2$, $Cu(CH_3COO)$, $CdCl_2$, $SnCl_2$, $GaCl_3$, $FeCl_3$, or Se into synthesis (Figure S6). Only the introduction of $CuCl_2$ and $Cu(CH_3COO)$ improved temporal response (Figure S7). $CuCl_2$ is stable in air and produces better

Figure 2. Morphology of In_2S_3 nanoplates during copper doping. STEM images of In_2S_3 products when (A) 1.0, (B) 2.7, and (C) 12.0 mg $CuCl_2$ were added into solution during postdoping. (D) HRTEM images of 2.7 mg $CuCl_2$-doped In_2S_3 nanoplates. White stars in panel C marked white spots on the edge of In_2S_3 nanoplates.

performance with high reproducibility, therefore we focus our investigation on the $CuCl_2$ doping results.

The most effective experimental protocol was one-pot postdoping which we now summarize. First, In_2S_3 is synthesized before doping and no isolation or purification is carried out. The resultant In_2S_3 nanoplates are doped by introducing $CuCl_2$ dissolved in oleylamine into the In_2S_3 solution vessel. The solution color changes from bright yellow to pink to red to dark red as more $CuCl_2$ is introduced. Drop-by-drop addition of $CuCl_2$ solution was found to produce the best results;[21] we propose that maintaining a low copper concentration in the solution facilitates the gradual incorporation of copper ions into In_2S_3 nanoplates and avoids nucleation of a new phase. As shown in Figure 2A,B, when less than 3 mg of $CuCl_2$ was added during this process, the size and morphology of In_2S_3 nanoplates were maintained. Figure 2D showed HRTEM image of copper-doped In_2S_3 nanoplate. Careful examination of several nanoplates showed continuous lattice fringes and no observation of second phase. When 12 mg $CuCl_2$ was applied in synthesis, an additional phase appeared on the edge of In_2S_3 nanoplates, as marked by white stars in Figure 2C. In this overdoping case, the integrity of In_2S_3 hexagonal nanoplates was partly destroyed, and they were converted into nanoplates with irregular shapes and saw-toothed edges. Excessive levels of Cu^{2+} result in competition with In^{3+} for S, resulting in formation of copper sulfide, similar to the cation exchange observed in the Ag_2S−CdS system.[22]
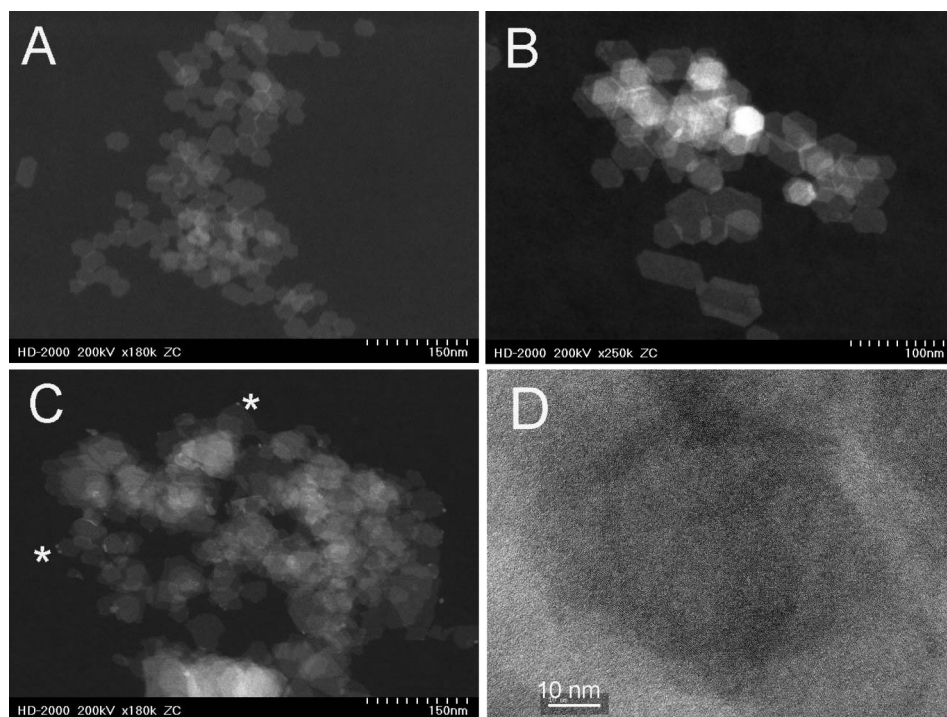
TABLE 1. Composition of Copper-Doped In₂S₃ Expected from Added Precursor and Calculated from ICP Results

	atomic percentage calculated from precursor			atomic percentage determined from ICP		
CuCl₂ added in synthesis	Cu	In	S	Cu	In	S
0 mg		40.0	60.0		42.3	57.7
1.1 mg	0.4	39.9	59.8	0.4	41.8	57.8
2.7 mg	0.9	39.7	59.5	0.9	41.9	57.2
12.0 mg	3.5	38.6	57.9	3.8	39.2	57.0

We carried out several experiments to ascertain whether copper was truly being incorporated into In₂S₃. We sought first to confirm the presence of copper in our sample: after 3 days of butylamine ligand exchange, a process that should remove dopant not incorporated into the bulk but instead loosely bound to the surface,[23,24] we carried out ICP-AES measurements. As summarized in Table 1, copper was detected in all samples, including ligand-exchanged materials, into which CuCl₂ had been added postsynthesis. In addition, the composition calculated from ICP results agreed very well with the value expected from added precursors, indicating nearly complete incorporation of copper into final products. We note sulfur content lies below its stoichiometric value in all samples, consistent with the n-type nature of our materials further discussed below.[20,25]

We then carried out powder XRD to investigate which crystalline phases were present in our synthetic products. As shown in Figure 3A, the XRD pattern of copper-doped sample showed characteristic peaks of tetragonal In₂S₃ (JCPDS 25-0390). We found evidence of no phase other than β-In₂S₃. The strong broad peak at 20° was also observed in InCl₃ and oleylamine mixture without any treatment: we associate this peak with the In³⁺-olelamine complex. Careful examination of the XRD patterns revealed no additional peaks associated with copper compounds such as CuO or Cu₂S. This finding, that a single phase was present, agreed with STEM observations discussed above that all nanoplates had the same contrast, as shown in Figure 2A and Figure 2B.

Taken together, these findings—that Cu is present in the samples (ICP-AES), but does not form a second phase (XRD and STEM)—suggest that the Cu is indeed incorporated into the In₂S₃ lattice.

We sought to investigate the state in which Cu dopants are in the lattice using electron paramagnetic resonance (EPR) investigation. EPR characterization of all our samples with 35 GHz Q-band at 77 K revealed no signal, indicating that Cu²⁺ is not present in our samples.[26] We conclude that copper exists as Cu⁺ in our samples, a finding that is supported by XPS data shown in Figure 3B. The binding energy of Cu 2p³/² is 932.7 eV in our sample, characteristic of monovalent copper.[27] We believe Cu²⁺ is reduced by oleylamine to Cu⁺ during the doping process. Oleyamine is widely used to reduce sulfur or selenium in sulfide[28] and selenide[29] Cu²⁺ to Cu⁺ in chalcopyrite nanocrystal[30] syn-

thesis, and Reihaneh Malakooti *et al*. proposed the amine group could be oxidized into a nitroso group.[31] However, the detailed reaction pathway is not clear yet.
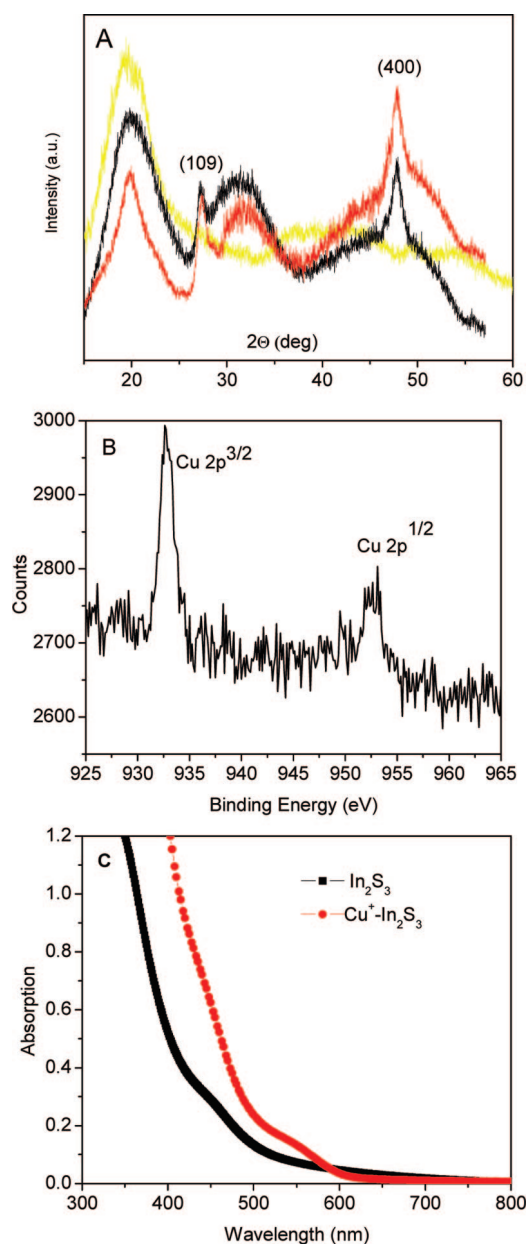

Figure 3. (A) XRD patterns of undoped In₂S₃ nanoplates (red), copper-doped In₂S₃ nanoplates (black), and InCl₃ and oleylamine mixture (yellow); (B) XPS spectrum of copper in copper-doped In₂S₃; (C) absorption spectra of undoped and doped In₂S₃ nanoplates in toluene solution.

As further evidence of Cu$^+$ incorporation, we note that the absorption spectrum of these materials shows a 50 nm shift in its onset following doping. Since quantum confinement is not at play in this material, this red shift is most likely a consequence of a bulk bandgap change instead of a surface effect. Co^{2+} doping in In$_2$S$_3$ has previously been reported to reduce the band gap of bulk In$_2$S$_3$ thin film from 1.98 to approximately 1.86 eV.[32] A similar shift appears to be at work in our Cu$^+$-doped In$_2$S$_3$ nanoparticles.

In summary, these data indicate that our In$_2$S$_3$ nanoplates are doped with Cu$^+$ at concentrations ranging from 0.4% to 0.9% (for 1.1 mg and 2.7 mg CuCl$_2$ in synthesis, respectively). Previous studies showed that for <2% Co^{2+}- and <4% Cu$^+$-doped In$_2$S$_3$ thin film,[33,34] the dopants located in the T_d symmetry site of the In$_2$S$_3$ host lattice, therefore we believe Cu$^+$ ions also fill into the intrinsic tetragonal vacancies in our In$_2$S$_3$ nanoplates. Diffuse reflectance measurements of Cu$^+$−In$_2$S$_3$ materials could further clarify the details of Cu$^+$ incorporation.[34]

We report in detail on the device performance of Cu$^+$-In$_2$S$_3$ nanoplate photodetectors in Figure 4. All measurements were carried out in air and the applied field is 2 V/μm. As shown in Figure 4A, 0.4% Cu$^+$-doped In$_2$S$_3$ device showed high responsivity (47.8 A/W) but slow temporal response (>1s), similar to the undoped In$_2$S$_3$ device. In contrast, 0.9% Cu$^+$-doped In$_2$S$_3$ showed dramatically improved performance: responsivity as high as 15 A/W, gain as high as 39, and temporal response (defined as time spent in 90% photocurrent decay) below 0.1 s were achieved simultaneously. Further increase of Cu$^+$ doping to 3.8% maintained fast response; however, it also was accompanied with decreased responsivity and undesired drift. All device performance is summarized in Table 2 for clear comparison.

We further characterized our best 0.9% Cu$^+$-doped In$_2$S$_3$ device. Figure 5A shows typical $I-V$ characteristics in the dark and under 7.4 uW/cm^2 illumination (λ = 470 nm). The gold electrode (E_F = 5.1 eV) and Cu$^+$−In$_2$S$_3$ film form a nonohmic contact as seen in the nonlinear $I-V$ near the origin. This is consistent with a large work function difference between Au (−5.2 eV) and n-type In$_2$S$_3$ (E_c = −3.8 eV and a Fermi energy a few tenths of an eV deeper in view of significant but nondegenerate doping).

The dependence of photocurrent on incident optical power, shown in Figure 5B, exhibits a power dependence of ~0.88, that is, $I_p \approx P^{0.88}$, suggestive of a sensitized photoconductor with a multiplicity of trap states.

We report the spectral responsivity of Cu$^+$−In$_2$S$_3$ in Figure 5C. The 50 nm red-shift of photoresponse onset for Cu−In$_2$S$_3$ device compared with undoped In$_2$S$_3$ closely follows the absorption spectral shift in solution seen in Figure 3C. The correspondence between optical absorbance and photodetector responsivity spectral
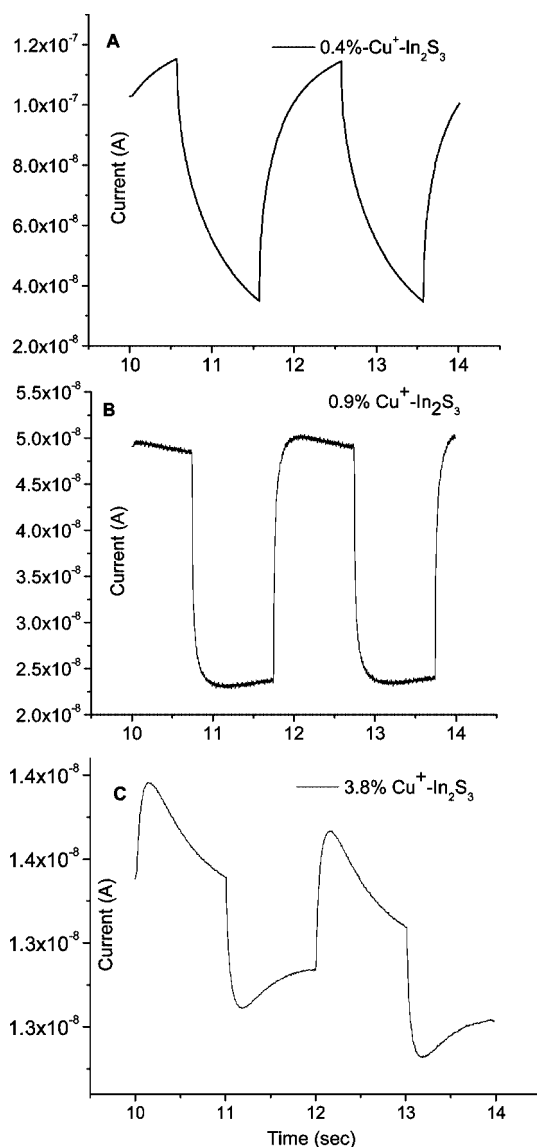

Figure 4. Temporal photoresponse of 0.4% Cu$^+$-doped In$_2$S$_3$ (A), 0.9% Cu$^+$-doped In$_2$S$_3$ (B), and 3.8% Cu$^+$-doped In$_2$S$_3$ (C) device to 470 nm monochromatic light illumination under optical intensity of 7.4 μW/cm^2.

shifts are also consistent with the successful incorporation of Cu$^+$ into the nanocrystals.

We also carried out photocurrent decay fitting to compare time constant of photoresponse in In$_2$S$_3$ and Cu−In$_2$S$_3$ photodetector. As shown in Figure 5D, the In$_2$S$_3$ photodetector showed two time constants of 0.96 and 11.0 s. In contrast, the Cu$^+$−In$_2$S$_3$ photodetector revealed a fast component with time constant of ~39 ms and a slower one of ~256 ms. This observation sug-

TABLE 2. Summary of Device Performance as a Function of Extent of Cu$^+$ Doping

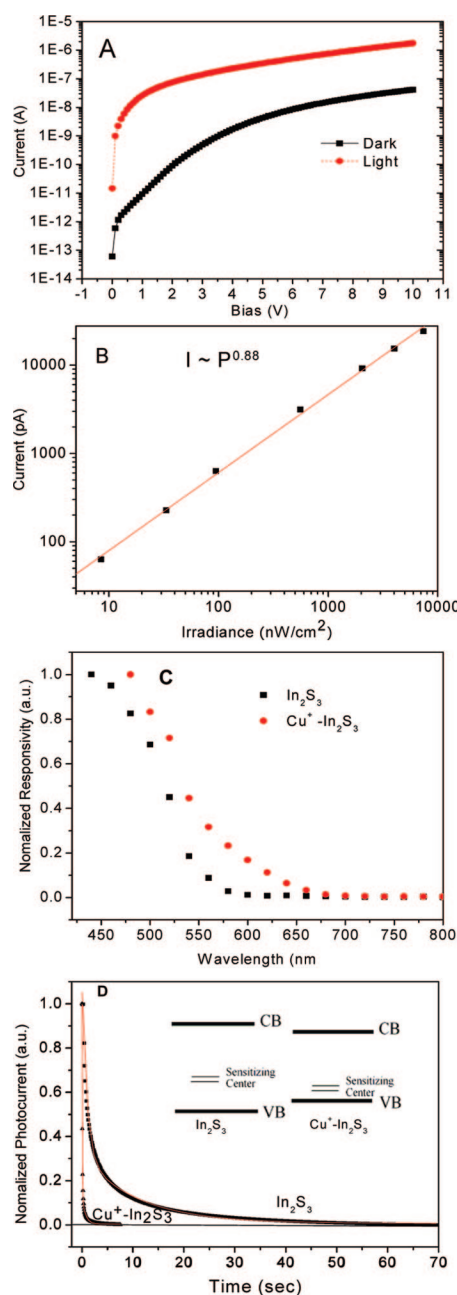| Cu$^+$ content (atom %)	Id (nA)	Il (nA)	R (A/W)	temporal response	gain
0.4%	35.4	79.7	47.8	>1 s	126.0
0.9%	23.8	24.7	14.8	~0.1 s	39.0
3.8%	12.8	0.8	0.5	~0.1 s	1.3

Figure 5. Optoelectronic characteristics of the 0.9% Cu^+-doped In_2S_3 photodetector. (a) Current−voltage characteristic of the photoconductive devices under dark and light conditions. (b) Measured photocurrent *versus* incident optical intensity, the photocurrent exhibits a sublinear dependence on optical power suggestive of sensitized photoconductivity. (c) Normalized spectral responsivity of In_2S_3 and Cu^+-In_2S_3 photodetector at 0.5 Hz modulation frequency and 2 V/µm applied electric field. (D) Exponential fitting of photocurrent decay of In_2S_3 and Cu^+−In_2S_3 photodetector. Inset showed the schematic diagram of proposed model for photoconductivity in In_2S_3 and Cu−-In_2S_3 photodetector.

gested that Cu^+ doping indeed improved device temporal response.

For photodetector application, responsivity and noise current should be jointly taken into account to yield specific (or normalized) detectivity D^* in unit of jones (cm $Hz^{1/2}$ W^{-1}). D^* is given as $(A\Delta f)^{1/2}R/i_n$, where

A is the effective area of the detector in cm^2, Δf is the electrical bandwidth in Hz, and R the responsivity in A/W measured under the same conditions as the noise current i_n in A. The measured dark current noise of our device at 10 Hz is ∼0.18 pA/$Hz^{1/2}$ resulting the D^* of 2.8 × 10^{11} jones.

DISCUSSION

We now discuss the flow of current and the origins of photoconductive gain in the devices reported herein.

In_2S_3 is reported to be n-type material;[20] our observed sulfur deficiency in all samples is consistent with this n-type behavior. Thus we present the photoconductive operation of these devices with reference to electron flow. Upon illumination, electron−hole pairs are created, and holes are rapidly captured to traps associated with the valence band. This trapping process extends the lifetime τ of both carrier types, and photogenerated electrons are thus able to flow for this lifetime. If the carrier lifetime exceeds the time for electrons to transit the device τ_t, photoelectrons can be extracted and reinjected within their lifetime: gain, defined as the ratio of extracted electrons to incident photons, or equivalently the ratio of carrier lifetime to transit time, may result. Our observed lifetime of 0.1 s combined with observed gain of 39 leads to our estimation of the transit time for electrons across the 5 um gap as 2.6 ms. From knowledge of the applied field, we are able to provide a lower-bound estimate of the electron mobility to be 9.6 × 10^{-4} cm^2/Vs. This lower-bound is obtained by assuming that the field is constant across the device.

In the In_2S_3 device, deep hole traps result in high gain and slow response. Cu^+ doping narrows the band gap of In_2S_3 and decreases the distance between valance band edge and traps depth. Traps are shallower in Cu^+−In_2S_3 and consequently produce devices with lower gain and higher speed. Even if the 0.2 eV band-gap contraction were evenly split between the bands, as much as an $exp(-0.1/kT) \approx$ 50-fold decrease in carrier lifetime can be accounted for through this effect (please refer to Supporting Information for details).

CONCLUSION

In summary, we reported the first solution-processed visible photodetector with high sensitivity and fast temporal response from Cu^+-doped In_2S_3 nanomaterials. This is the first demonstration of a In_2S_3 visible-wavelength photodetector. The undoped In_2S_3 device showed hundreds of A/W for responsivity but slow response. By taking advantage of their intrinsic vacancies, we successfully doped In_2S_3 with Cu^+ in solution and significantly improved device speed to response time of around 0.1 s. Low toxicity, solution-processed capability, high responsivity, and reasonable speed make our Cu^+-In_2S_3 photodetector a strong candidate for many potential applications.

METHODS

In$_2$S$_3$ and Cu$^+$—In$_2$S$_3$ Nanoplates Synthesis. All chemicals used were purchased from Sigma-Aldrich. Oleylamine was pumped with a Schlenk line at 80 °C for 1 day, butylamine was distilled before use. All other materials were used without further purification. Synthesis was conducted under inert atmosphere using a Schlenk line and isolated in a glovebox. Synthesis of In$_2$S$_3$ nanoplates is described elsewhere.[19] For Cu$^+$—In$_2$S$_3$ nanoplates, we first mixed 1 mmol InCl$_3$, 1.5 mmol sulfur powder, and 10 mL of oleylamine and pumped at 120 °C for 1 h to produce a clear brown solution. Afterward N$_2$ was introduced into the reacting vessel and heated the solution to 215 °C and incubated for 1 h to produce In$_2$S$_3$ nanoplates. Then a given amount of CuCl$_2$ dissolved in 5 mL oleylamine was injected into the flask drop by drop with syringe. This injection process lasted for 40 min and the solution color changed from yellow to red. After injection, the solution was maintained at 215 °C for another 40 min. After cooling naturally to room temperature, the flask was sealed and transferred into glovebox for isolation. The raw solution was washed first by toluene and precipitated by methanol, and repeated this process twice. Finally the precipitates were collected and dried for ligand exchange.

Ligand Exchange, Device Fabrication, and Treatment. Butyamine ligand exchange and device produce were done at inert atmosphere in a glovebox. Typically we dispersed all sediments collected during isolation into 10 mL of distilled butylamine and stored them undisturbed for 2 days. Afterward In$_2$S$_3$ nanomaterials were precipitated by methanol and redispersed in 5 mL of toluene to produce concentrated solution. Photodetector was fabricated by dropping 10 μL of such solution onto precleaned interdigitated gold electrodes and dried naturally. When the device was ready, we transferred it into vacuum oven (preheated to 200 °C) and annealed under vacuum for 10 min. Device was measured in air.

Characterization. Visible—near-NIR absorption spectra of the nanomaterials in toluene were recorded at room temperature using a Cary 500 UV—vis—near-IR spectrophotometer. FTIR spectra were obtained using a Bruker Tensor 27 infrared spectrometer. Samples were prepared by drop-casting the same volume of In$_2$S$_3$ toluene solution before and after butyalmine ligand exchange onto KBr substrates, after which the samples were dried in air and produced films with approximately identical thickness. XRD was recorded with a Siemens diffractemeter with Cu Kα radiation (λ = 1.54178 Å). ICP measurements were performed using a Perkin-Elmer model Optima 3000DV ICP AEOS. XPS was recorded at a PHI 5500 (XPS) spectrometer. Samples were prepared by drop-casting nanoparticle from toluene onto gold film sputtered on top of undoped silicon wafer. EPR was done on Varian E-9 EPR multifrequency spectrometer using 35 GHz Q-band at 77 K. The size and morphology of as-synthesized samples were characterized on Hitachi HD-2000 scanning transmission electron microscopy. We prepared the sample by putting one drop of In$_2$S$_3$ or Cu—-In$_2$S$_3$ toluene solution onto 300 mesh carbon/Formvar copper grid. HRTEM images were taken on Titan TM 80-300 using holey carbon film on Ni grid as substrate. SEM characterization was done on Hitachi S-5200 scanning electron microscopy. SEM sample was prepared by drop-casting In$_2$S$_3$ solution onto clean ITO substrate. Film thickness was measured with a Veeco Dektak3 surface profiler.

All current—voltage measurements were taken with an Agilent 4155C semiconductor parameter analyzer. The device was top-illuminated using an overhead blue LED operating at 470 nm. Optical intensity was measured with a Melles-Griot broadband power meter. The active device area was fixed as 0.015 mm^2 throughout the whole experiments. Dark current noise in the photodetectors was measured using a Stanford Research SR830 lock-in amplifier. The devices were biased using alkaline batteries at 10 V and testing was carried out in an electrically shielded and optically sealed probe station on a floating table to minimize vibrational noise. Knowing device area, responsivity, and the noise current normalized to the measurement bandwidth, we were able to obtain the D^* normalized detectivity value of our device as reported in the text.

Supporting Information Available: SEM characterization of In2S3 film, details of many "failed" examples of trap manipulation as well as theoretical calculation of change of trap activation energy after Cu$^+$-doping. This material is available free of charge *via* the Internet at http://pubs.acs.org.

REFERENCES AND NOTES

1. Konstantatos, G.; Howard, I.; Fischer, A.; Hoogland, S.; Clifford, J.; Klem, E.; Levina, L.; Sargent, E. H. Ultrasensitive Solution-Cast Quantum Dot Photodetectors. *Nature* **2006**, *442*, 180–183.

2. Konstantatos, G.; Clifford, J.; Levina, L.; Sargent, E. H. Sensitive Solution-Processed Visble Wavelength Photodetectors. *Nat. Photon.* **2007**, *1*, 531–534.

3. Qi, D. F.; Fischbein, M.; Drndic, M.; Selmic, S. Efficient Polymer-Nanocrystal Quantum-Dot Photodetectors. *Appl. Phys. Lett.* **2005**, *86*, 093103-1–093103-3.

4. Oertel, D. C.; Bawendi, M. G.; Arango, A. C.; Bulovic, V. Photodetectors Based on Treated CdSe Quantum-Dot Films. *Appl. Phys. Lett.* **2005**, *87*, 213505-1–213505-3.

5. Dindar, A.; Therrien, J. A Resonant Tunneling CdSe Quantum Dot Photodetector for Spectral Resolution in the Visible Region. *Proc. SPIE* **2007**, *6479*, 64790U1–64790U8.

6. Amos, F. F.; Morin, S. A.; Streifer, J. A.; Hamers, R. J.; Jin, S. Photodetector Arrays Directly Assembled onto Polymer Substrates from Aqueous Solution. *J. Am. Chem. Soc.* **2007**, *129*, 14296–14302.

7. Yotter, R. A.; Wilson, D. M. A Review of Photodetectors for Sensing Light-Emitting Reporters in Biological Systems. *IEEE Sens. J.* **2003**, *3*, 288–303.

8. Fossum, E. R. Digital Camera System on a Chip. *IEEE Micro* **1998**, *18*, 8–15.

9. Jin, Y.; Wang, J.; Sun, B.; Blakesley, J. C.; Greenham, N. C. Solution-Processed Ultraviolet Photodetectors Based on Colloidal ZnO Nanoparticles. *Nano. Lett.* **2008**, *8*, 1649–1653.

10. Konstantatos, G.; Levina, L.; Fischer, A.; Sargent, E. H. Engineering the Temporal Response of Photoconductive Photodetectors *via* Selective Introduction of Surface Trap States. *Nano Lett.* **2008**, *8*, 1446–1450.

11. Urban, J. J.; Talapin, D. V.; Shevchenko, E. V.; Kagan, C. R.; Murray, C. B. Synergism in Binary Nanocrystal Superlattices Leads to Enhanced p-type Conductivity in Self-Assembled PbTe/Ag$_2$Te Thin Films. *Nat. Mater.* **2007**, *6*, 115–121.

12. Talapin, D. V.; Murray, C. B. PbSe Nanocrystal Solids for n- and p-Channel Thin Film Field-Effect Transistors. *Science* **2005**, *310*, 86–89.

13. Coe, S.; Woo, W. K.; Bawendi, M.; Bulovic, V. Electroluminescence from Single Monolayers of Nanocrystals in Molecular Organic Devices. *Nature* **2002**, *420*, 800–803.

14. Gur, I.; Fromer, N. A.; Geier, M. L.; Alivisatos, A. P. Air-Stable All-Inorganic Nanocrystal Solar Cells Precessed from Solution. *Science* **2005**, *21*, 462–465.

15. Luther, J. M.; Law, M.; Beard, M. C.; Song, Q.; Reese, M. O.; Ellingson, R. J.; Nozik, A. J. Schottky Solar Cells Based on Colloidal Nanocrystal Films. *Nano Lett.* **2008**, *8*, 3488–3492.

16. Jayakrishnan, R.; John, T. T.; Kartha, C. S.; Vijayakumar, K. P.; Jain, D.; Chandra, L. S. S.; Ganesan, V. Do the Grain Boundaries of β-In2S3 Thin Films Have a Role in Sub-

Band-Gap Photosensitivity to 632.8 nm. *J. Appl. Phys.* **2008**, *103*, 053106-1–053106-6.

17. Norris, D. J.; Efros, A. L.; Erwin, S. C. Doped Nanocrystals. *Science* **2008**, *319*, 1776–1779.

18. Dalpian, G. M.; Chelikowsky, J. R. Self-Purification in Semiconductor Nanocrystals. *Phys. Rev. Lett.* **2006**, *96*, 226802-1–226802-4.

19. Park, K. H.; Jang, K.; Son, S. U. Synthesis, Optical Properties, and Self-Assembly of Ultrathin Hexagonal In_2S_3 Nanoplates. *Angew. Chem., Int. Ed.* **2006**, *45*, 4608–4612.

20. Rehwald, W.; Harbeke, G. On the Conduction Mechanism in Single Crystal β-Indium Sulfide In_2S_3. *J. Phys. Chem. Solid* **1965**, *26*, 1309–1318.

21. Mixed $InCl_3$, $CuCl_2$, and sulfur powder at the beginning and then cooked also produced copper-doped In_2S_3 but with large size and morphology distribution. Direct injection of $CuCl_2$ solution into the reaction vessel rendered a sudden burst of copper concentration in solution, leading to porous copper-doped In_2S_3 nanoplates.

22. Son, D. H.; Hughes, S. M.; Yin, Y. D.; Alivisatos, A. P. Cation Exchange Reactions in Ionic Nanocrystals. *Science* **2004**, *306*, 1009–1012.

23. Mikulec, F. W.; Kuno, M.; Bennati, M.; Hall, D. A.; Griffin, R. G.; Bawendi, M. G. Organometallic Synthesis and Spectroscopic Characterization of Manganese-Doped CdSe Nanocrystals. *J. Am. Chem. Soc.* **2000**, *122*, 2532–2540.

24. Nag, A.; Chakraborty, S.; Sarma, D. D. To Dope Mn^{2+} in a Semiconducting Nanocrystal. *J. Am. Chem. Soc.* **2008**, *130*, 10605–10611.

25. John, T. T.; Bini, S.; Kashiwaba, Y.; Abe, T.; Yasuhiro, Y.; Kartha, C. S.; Vijayakumar, K. P. Characterization of Spray Pyrolysed Indium Sulfide Thin Films. *Semicond. Sci. Technol.* **2003**, *18*, 491–500.

26. Massa, M. B.; Dalosto, S. D.; Ferreyra, M. G.; Labadie, G.; Calvo, R. Vibronic Behavior and Single-Crystal EPR Spectra of Cu(II) in Copper-Doped Diaqua(ʟ-aspartato)zinc(II) Hydrate. *J. Phys. Chem. A* **1999**, *103*, 2606–2617.

27. NIST X-ray Photoelectron Spectroscopy Database, http://srdata.nist.gov/xps/ (accessed October, 2008).

28. Joo, J.; Na, H. B.; Yu, T.; Yu, J. H.; Kim, Y. W.; Wu, F. X.; Zhang, J. Z.; Hyeon, T. Generalized and Facile Synthesis of Semiconducting Metal Sulfide Nanocrystals. *J. Am. Chem. Soc.* **2003**, *125*, 11100–11105.

29. Park, K. H.; Jang, K. J.; Kim, S. Y.; Kim, H. J.; Son, S. K. Phase-Controlled One-Dimensional Shape Evolution of InSe Nanocrystals. *J. Am. Chem. Soc.* **2006**, *128*, 14780–14781.

30. Tang, J.; Hinds, S.; Kelley, S. O.; Sargent, E. H. Synthesis of Colloidal $CuGaSe_2$, $CuInSe_2$, and $Cu(InGa)Se_2$ Nanoparticles. *Chem. Mater.* **2008**, *20*, 6906–6910.

31. Malakooti, R.; Cademartiri, L.; Akcakir, Y.; Petrov, S.; Migliori, A.; Ozin, G. A. Shape-Controlled Bi_2S_3 Nanocrystals and Their Plasma Polymerization into Flexible Films. *Adv. Mater.* **2006**, *18*, 2189–2194.

32. Kim, C. D.; Lim, H.; Park, H. L.; Park, H. Y.; Kim, J. E.; Kim, H. G.; Kim, Y. G.; Kim, W. T. Optical Absorption of Co^{2+} ions in In_2S_3 Thin Films. *Thin Solid Films* **1993**, *224*, 69–73.

33. Kim, W. T.; Lee, W. S.; Chung, C. S.; Kim, C. D. Optical Properties of In_2S_3:Co^{2+} Single Crystals. *J. Appl. Phys.* **1988**, *63*, 5472–5475.

34. Py, F.; Womes, M.; Durand, J. M.; Olivier-Fourcade, J.; Jumas, J. C. Copper in In_2S_3: A Study by X-ray Diffraction, Diffuse Reflectance and X-ray Absorption. *J. Alloys Compd.* **1992**, *178*, 297–304.